

Multi-node Acceleration for Large-scale GCNs

Gongjian Sun, Mingyu Yan, Duo Wang, Han Li, Wenming Li,
Xiaochun Ye, Dongrui Fan, *Senior Member, IEEE* and Yuan Xie, *Fellow, IEEE*

Abstract—Limited by the memory capacity and computation power, single-node graph convolutional neural network (GCN) accelerators cannot complete the execution of GCNs within a reasonable time, due to explosive graphs nowadays. Thus, large-scale GCNs call for a multi-node acceleration system (MultiAccSys) like TPU-Pod for large-scale neural network. In this work, we aim to scale the single-node GCN accelerator to accelerate GCNs on large-scale graphs. We first identify the communication pattern and challenges of the multi-node acceleration for GCNs on large-scale graphs. We observe that (1) the existence of the irregular coarse-grained communication pattern exists in the execution of GCNs in MultiAccSys, which introduces massive redundant network transmissions and off-chip memory accesses; (2) the acceleration of GCNs in MultiAccSys is mainly bounded by network bandwidth but tolerates network latency. Guided by the above observations, we then propose MultiGCN, an efficient MultiAccSys for large-scale GCNs that trades network latency for network bandwidth. Specifically, by leveraging the network latency tolerance, we *first* propose a topology-aware multicast mechanism with a one put per multicast message-passing model to reduce transmissions and alleviate network bandwidth requirements. *Second*, we introduce a scatter-based round execution mechanism which cooperates with the multicast mechanism and reduces redundant off-chip memory accesses. Compared to the baseline MultiAccSys, MultiGCN achieves 4~12 \times speedup using only 28%~68% energy, while reducing 32% transmissions and 73% off-chip memory accesses on average. Besides, MultiGCN not only achieves 2.5~8 \times speedup over the state-of-the-art multi-GPU solution, but also can scale to large-scale graph compared to single-node GCN accelerator.

Index Terms—Deep learning, graph neural network, hardware accelerator, multi-node system, communication optimization.

1 INTRODUCTION

GRAPH Convolutional Neural Networks (GCNs) have emerged as a premier paradigm to address the graph learning problem via generalizing the information encoding to graph topologies that can represent extremely complicated relationships [1]–[5]. In reality, GCNs have been widely applied in many critical fields such as knowledge inference [6], recommendation system [7], visual reasoning [8], traffic prediction [9], EDA [10], and GCN workloads can be found at many data centers [1], [9].

GCNs typically exhibit a hybrid execution pattern introduced by the two following distinct execution phases, which hinder the acceleration of GCNs in GPUs [11], [12]. The *Aggregation* phase traverses all vertices and aggregates the feature vectors of neighboring vertices into the current vertex, presenting an irregular execution pattern like graph processing (GP). The *Combination* phase further transforms the feature vector of each vertex into a new one using a multi-layer perceptron (MLP), exhibiting a regular execution pattern like neural network (NN). Such execution patterns hinder the acceleration of GCNs in GPUs which are inherently optimized for compute-intensive workloads with regular execution pattern [13].

To tackle this hybrid execution pattern, previous efforts [11], [14]–[17] propose a series of single-node GCN accelerators. Although these accelerators have achieved great improvement on both performance and energy efficiency compared with GPUs, they suffer two following inefficiencies in the processing of large-scale GCNs. *First*, with limited hardware resources in categories

such as compute and buffer, a single-node accelerator cannot complete the execution of large-scale GCNs within a reasonable time, not to mention that the scales of real-world graphs keep growing rapidly [1], [18]. *Second*, massive time and energy have to be taken to move data between memory and hard disk [1], because single-node accelerators lack of memory to accommodate the whole data of large-scale graph. Thus, a multi-node acceleration system (MultiAccSys) is highly desired for large-scale GCNs.

Previous efforts propose a series of MultiAccSyses for NNs and GPs, achieving great improvements on both performance and energy efficiency. However, they fail to tackle the unique execution pattern in the multi-node acceleration of GCNs. MultiAccSyses for NNs, e.g., TPU-Pod [19], tailor their hardware datapath to the regular execution pattern such as coarse-grained regular communication pattern inter-node, to leverage the regularity for high performance of large-scale NN acceleration. Similarly, MultiAccSyses for GPs, e.g., Tesseract [20], tailor their hardware datapath to the irregular execution pattern of GPs such as fine-grained irregular communication pattern inter node, to alleviate the irregularity for high performance of large-scale GP acceleration. Unfortunately, the multi-node acceleration for GCNs exhibits distinct execution patterns, i.e., the coarse-grained irregular communication inter node and hybrid execution pattern intra node. Such execution patterns make GCNs ill-suited to be accelerated by previous MultiAccSyses which are elaborately tailored to different ones.

In this paper, we aim to scale the single-node accelerator to accelerate GCNs on large-scale graphs like TPU-Pod [19], since the performance and energy efficiency of single-node GCN accelerators are significantly higher than that of high-end GPUs. To identify the unique execution pattern and the challenges of the multi-node acceleration for GCNs, we characterize the execution of large-scale GCNs in a straightforward design of MultiAccSys for GCNs as shown in Figure 1(a). To ensure an effective

- G. Sun, M. Yan, D. Wang, H. Li, W. Li, X. Ye, D. Fan are with the Institute of Computing Technology, Chinese Academy of Sciences, Beijing, China (Email: {sungongjian19s, yanmingyu, wangduo18z, lihan-ams, liwenming, yexiaochun, fandr}@ict.ac.cn). G. Sun, M. Yan, D. Wang, H. Li, W. Li, D. Fan are also with University of Chinese Academy of Sciences, Beijing, China. Y. Xie is with University of California, Santa Barbara, California, USA (Email: yuanxie@ece.ucsb.edu). Corresponding author is M. Yan.

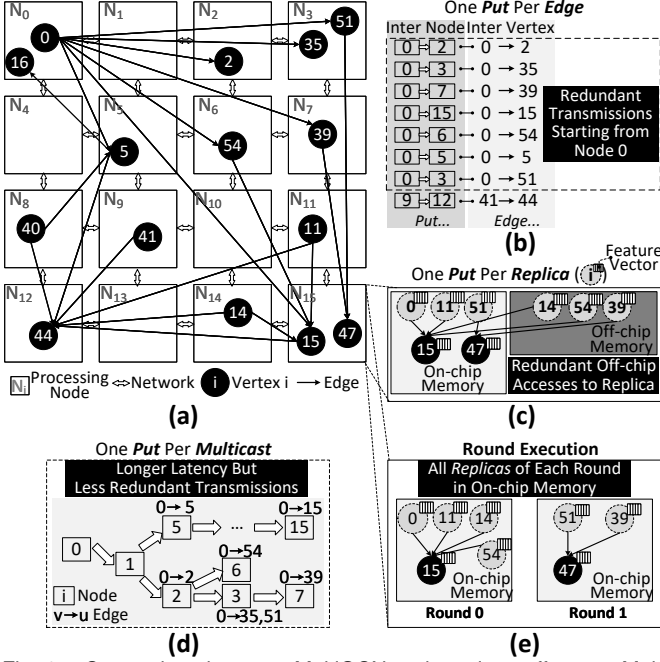


Fig. 1. Comparison between MultiGCN and previous efforts on MultiAccSys for graph processing: (a) Examples of graph and MultiAccSys for GCNs; (b) Disadvantage of MultiAccSys with one put per edge message-passing model; (c) Disadvantage of MultiAccSys with one put per replica message-passing model; (d) and (e) Advantage of MultiGCN based on one put per multicast message-passing model and scatter-based round execution.

characterization, we borrow a well-designed single-node GCN accelerator [11] to design the processing node and a representative message-passing model to alleviate the irregular communication pattern inter node, i.e., one put per edge (OPPE) [20]. We observe the existence of the irregular coarse-grained communication pattern exists in the execution of GCNs in MultiAccSys, which introduces massive redundant network transmissions and off-chip memory accesses. This communication pattern derives from the fact that (1) each transmission between nodes contains a long feature vector of neighbor vertex and (2) it is unpredictable when and to where it needs to be sent due to the irregular connection pattern of neighbors. As a result, the OPPE message-passing model causes many redundant coarse-grained transmissions because the long feature vector of each vertex must be repeatedly sent to all of its neighboring vertices, while many of which may be sent to or pass through the same processing node. For example, Figure 1(b) shows that the feature vector of vertex V_0 in the processing node N_0 is sent to neighboring vertices $V_2, V_{35}, V_{51}, V_{39}$... in processing nodes N_2, N_3, N_3, N_7 ..., respectively. To reduce these redundant transmissions, a one put per replica (OPPR) message-passing model is proposed [21], which only puts one replica of the feature vector to each processing node and shares it with all neighboring vertices in that processing node. However, the size of the replicas makes it difficult to store thousands of replicas on-chip, which inevitably leads to massive off-chip memory accesses. For example, Figure 1(c) shows that vertices V_{15} and V_{47} in the processing node N_{15} require accesses to the replicas of V_{14}, V_{54} , and V_{39} , which were previously received and stored off-chip because on-chip memory had been exhausted.

In light of the above challenges, we propose MultiGCN, an efficient MultiAccSys that accelerates the inference phase of large-scale GCNs by trading network latency for network bandwidth. *First, a topology-aware multicast mechanism with a one put*

per multicast message-passing model is proposed to alleviate network bandwidth requirements. As shown in Figure 1(d), by leveraging the latency tolerance we identified in the execution of GCNs as well as the known network and graph topologies, V_0 's feature vector is multicast in the transmission to reduce redundant transmissions. *Second, a scatter-based round execution mechanism is proposed to cooperate with the multicast mechanism, which inherently matches the behaviour of multicast.* Specifically, each processing node scatters the replicas of vertices' feature vectors to remote processing nodes which perform aggregation for their neighboring vertices. Besides, to reduce redundant off-chip memory accesses, the graph is partitioned into a certain number of sub-graphs, each for one execution round, as shown in Figure 1(e). Thus, all replicas of round 0 (i.e., V_0, V_{11}, V_{14} , and V_{54}) and round 1 (i.e., V_{51} and V_{39}) from remote processing nodes can be stored on-chip until the corresponding round completes. Intra- and inter-round overlap are utilized for higher performance.

The key contributions of this paper are as follows:

- We identify the communication pattern and challenges of multi-node acceleration for large-scale GCNs and observe that: (1) The irregular coarse-grained communication pattern exists and causes massive redundant transmissions and off-chip memory accesses; (2) Execution of GCNs in MultiAccSys is mainly bounded by network bandwidth but tolerates network latency.
- Accordingly, we propose an efficient MultiAccSys that accelerates the inference phase of large-scale GCNs by trading network latency for network bandwidth.
- We propose a topology-aware multicast mechanism to reduce redundant transmissions and alleviate network bandwidth requirements, along with a scatter-based round execution mechanism that cooperates with the multicast mechanism and reduces off-chip memory accesses.
- We implement MultiGCN in both RTL and cycle-accurate simulator to demonstrate its advance. Compared with OPPE-based MultiAccSys, MultiGCN achieves 4~12 \times speedup, and reduces 32% network transmissions as well as 73% off-chip memory accesses on average. Besides, MultiGCN achieves 2.5~8 \times speedup over the multi-GPU solution and can scale to large-scale graph compared to single-node GCN accelerator.
- We explore the design of MultiGCN in detail and provide insights into the relationships between hardware parameters, graph characteristics, and architecture techniques.

TABLE 1
Notations used in this paper.

| Notation | Explanation |
|-----------------------|---|
| $G = (V, E)$ | directed graph G |
| $V(V)$ | (size of) vertex set of graph G |
| $E(E)$ | (size of) edge set of graph G |
| (i, j) or $e_{i,j}$ | edge from vertex i to vertex j |
| d_v | incoming degree of vertex v |
| N_v | incoming neighbor set of vertex v |
| $h_v^k(h_v^k)$ | (length of) feature vector of vertex v at k -th layer |
| a_v^k | aggregated result of vertex v at k -th layer |

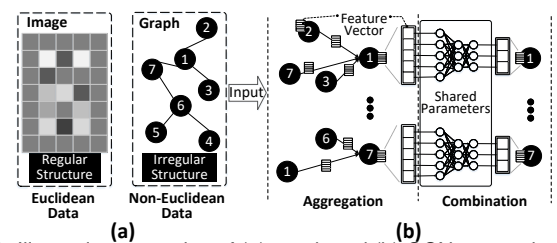


Fig. 2. Illustration examples of (a) graph and (b) GCNs execution.

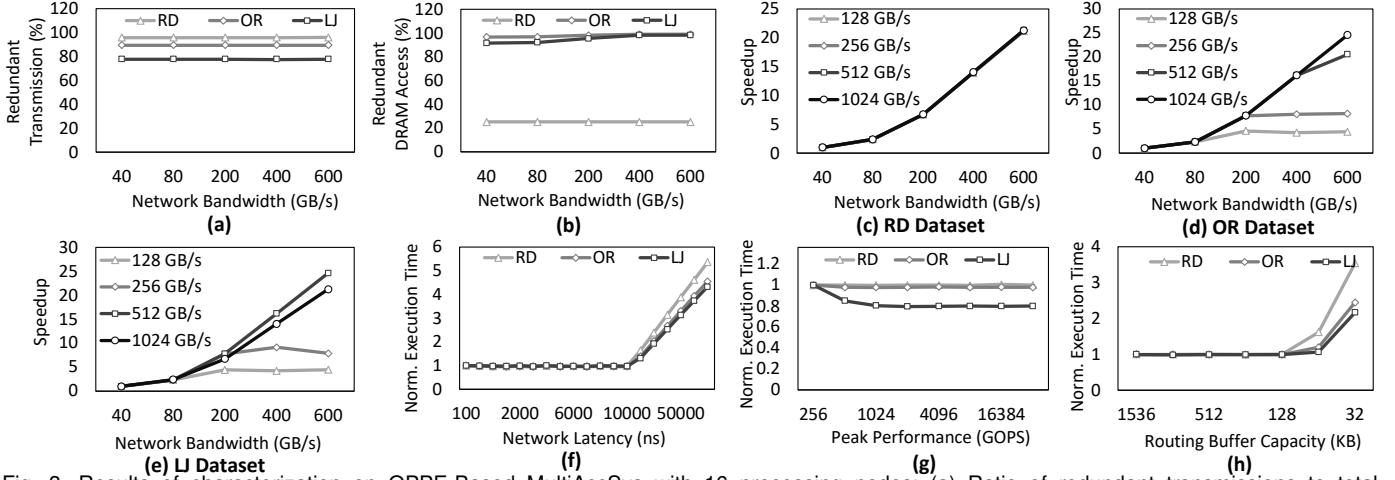


Fig. 3. Results of characterization on OPPE-Based MultiAccSys with 16 processing nodes: (a) Ratio of redundant transmissions to total transmissions across different network bandwidths; (b) Ratio of redundant DRAM accesses to total DRAM accesses across different network bandwidths; Speedup of GCN across different network bandwidths (X-axis) and DRAM bandwidths (4 Lines) on (c) RD, (d) OR, and (e) LJ datasets; Normalized execution time across (f) different network latencies, (g) different peak performances, and (h) different routing buffer capacities.

2 BACKGROUND

GCNs. Fig. 2 shows that typical GCNs take non-euclidean data as input, i.e., graphs which have irregular structure and differ to the images which have regular structure as shown in Fig. 2(a). GCNs consist of several graph convolutional layers, each with two main phases: *Aggregation* and *Combination*, which are formulated as Equation 1 using the notation in Table 1. For clarity, by “node” we refer to the processing node in MultiAccSys, and by “vertex” we refer to the element of the graph vertex set.

$$\forall v \in V \quad a_v^k = \text{Aggregate} \left(h_u^{k-1} \right)_{u \in \{v\} \cup N_v}, h_v^k = \text{Combine} \left(a_v^k \right). \quad (1)$$

In the k -th layer, for each vertex v , the feature vectors h_u^{k-1} of neighboring vertices in the N_v are aggregated into a_v^k following the graph topology by aggregate function in *Aggregation* phase, as shown in Fig. 2(b). Since *Aggregation* phase heavily relies on the graph structure that is inherently random and sparse, it suffers from irregular data communication. The *combine* function further transforms a_v^k to generate h_v^k using an MLP in *Combination* phase. All vertices use the same MLP to perform combine function, which results in intensive computation and high-degree data locality in *Combination* phase. The length of feature vector h_v^k is long and determined by the input dataset or the number of the MLP’s output neurons, up to thousands in the initial feature vectors h_v^0 of all vertices.

Network and Message-passing Model. Multi-node acceleration becomes an inevitable trend due to the ever-increasing demand on computation and storage capability in emerging domains such as deep learning [22]. High-speed network interface and network topology are the basic of multi-node acceleration. Network interface includes NVLink for GPU interconnection, PCIe for CPU and GPU interconnection, and so on. Network latency is a metric used to evaluate how much time consumed by the network interface to send a minimum packet from the source to the destination. Network topology includes star, bus, mesh, torus, and so on. For example, NVIDIA HGX incorporates 16 H100 GPUs together using NVLink and NVSwitch to build a star topology¹. Network bandwidth inter GPUs achieves 900GB/s. The message-passing model determines the transfer mode of MultiAccSys, such as the OPPE and OPPE models used in the MultiAccSys of GPs. For each vertex, the OPPE model sends one replica of the feature

vector to each neighboring vertex, while OPPE model only sends one replica of the feature vector to each processing node and shares it with all neighboring vertices in that processing node.

3 MOTIVATION

Inefficiencies of Single-node GCN Accelerators. Previous efforts propose several single-node accelerators for GCN acceleration, achieving significant improvement in both performance and efficiency compared with GPUs. However, the large and ever-growing scale of graphs hinder the efficient execution of GCNs on single-node accelerators. For example, HyGCN [11] proposes a hybrid architecture for GCNs to tackle the hybrid execution pattern, achieving average $6.5\times$ speedup with $10\times$ energy reduction over high-end GPUs. However, with limited off-chip memory bandwidth, on-chip buffer, and compute resources, a single-node accelerator cannot process large-scale GCNs within a reasonable time, let alone that the scale of real-world graphs continuously grows rapidly [1], [18]. In addition, large-scale graphs demand massive memory, which is hard to satisfy in a single-node accelerator [1], resulting in massive time and energy being continuously taken to move data between memory and hard disk. Thus, a MultiAccSys for GCNs is highly desired.

Inefficiencies of NN and GP MultiAccSyses. Previous efforts propose a series of MultiAccSyses for large-scale NNs and GPs, however, they fail to tackle the unique execution pattern of the multi-node acceleration for GCNs. For an example, TPU-Pod [19], its designers elaborately customize an MultiAccSys for NNs using an inter-node network interface like NVLink to connect many TPU chips together. Although TPU-Pod deliver near-linear speedup for the acceleration of large-scale NNs, the irregular coarse-grained communication pattern and hybrid execution pattern make GCNs ill-suited to be accelerated by previous MultiAccSyses which are elaborately tailored to the regular coarse-grained communication pattern and regular execution pattern. For another example, Tesseract [20], its designers elaborately customize an MultiAccSys for GPs using an well-designed message passing model (i.e., OPPE) to alleviate the fine-grained irregular communication pattern. Tesseract achieves great improvements in the acceleration of large-scale GPs, however, massive redundant coarse-grained transmissions are caused by the irregular coarse-grained communication pattern. Although the redundant transmissions can be reduced

1. <https://www.nvidia.cn/data-center/hgx/>

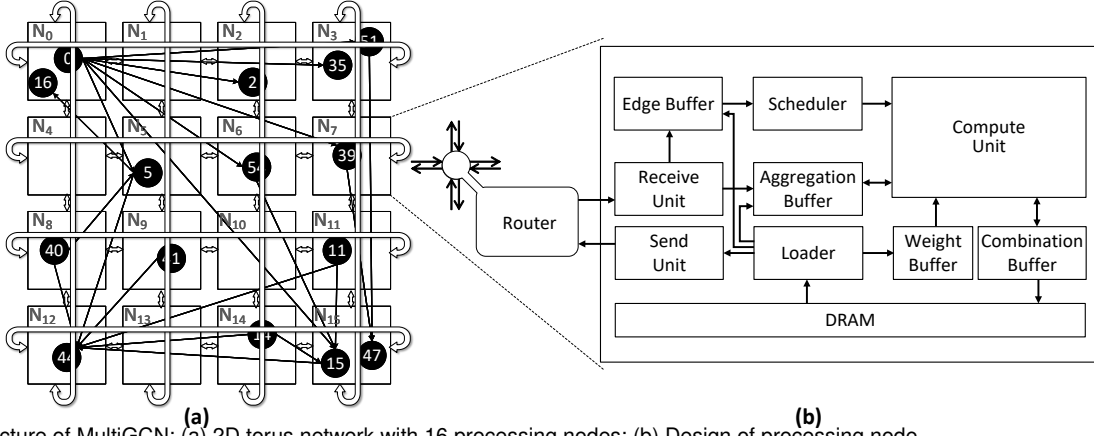


Fig. 4. Architecture of MultiGCN: (a) 2D torus network with 16 processing nodes; (b) Design of processing node.

by OPPER message-passing model [21], however, the size of the replicas of feature vectors makes it difficult to store thousands of replicas on-chip, which inevitably leads to massive off-chip memory accesses, let alone the hybrid execution pattern.

Characterization on A Straightforward Design. To identify the communication pattern and challenge of the multi-node acceleration for GCNs, a detailed characterization is conducted and results are shown in Figure 3. The processing node in this MultiAccSys is a variant of the single-node GCN accelerator of previous work [11] which elaborately tackle the hybrid execution pattern of GCNs. The message-passing model used in this MultiAccSys is inspired by OPPE model, which aims to tackle the irregular communication pattern caused by the irregular structure of graph topology. See Section 5 for our detailed evaluation methodology.

We observe that the irregular coarse-grained communication pattern exists in the execution of GCNs in MultiAccSys, which introduces massive redundant network transmissions and off-chip memory accesses. The irregular coarse-grained communication pattern is caused by two following reasons. (1) Each transmission between node contains a long-length feature vector of neighbor vertex, with up to hundreds of elements, determined by the length of input dataset or the number of the MLP’s output neurons. (2) It is unpredictable when and to where it needs to be sent due to the irregular connection pattern of neighbors in graph. As depicted in Figure 3(a) and (b), we observe that a vast range of redundant transmissions and DRAM accesses, ranging from 78% to 96% and 25% to 99.9%, respectively. This is because the long feature vector of each vertex must be repeatedly sent to all of its neighboring vertices, while many of which may be sent to or through the same processing node. In addition, received feature vectors need to be saved to DRAM upon receipt and loaded in DRAM while in use due to the large number of long feature vectors and limited on-chip cache capacity. These redundancies not only require additional network bandwidth and DRAM bandwidth, but also cause wasteful and unnecessary cost, which significantly hinders the performance and efficiency on MultiAccSys for GCNs.

We also observe that the acceleration of GCNs in MultiAccSys is mainly bounded by network bandwidth but tolerates network latency. Figure 3(c), (d), and (e) show that the speedup across different datasets grows almost linearly as network bandwidth increases when the DRAM bandwidth is sufficient (i.e., greater than 256 GB/s). This is because neighboring feature vectors with hundreds of elements for each vertex need to be sent and aggregated in a target processing node, following the irregular neighbor connection in *Aggregation* phase, which consumes much network bandwidth for better performance. However, Figure 3(f)

shows that the normalized execution time is nearly constant under different network latencies until which becomes around 20,000 ns. This value mainly relies on the processing time which is positively correlated with the length of feature vector and negatively correlated with the DRAM bandwidth of the processing node. This is because the received feature vectors is frequently store to or load from DRAM as aforementioned. Figure 3(g) shows that the normalized execution time is nearly constant under different peak performance when which is more than 1024 giga operations per second (GOPS). This is because the low utilization of network bandwidth and DRAM bandwidth become the performance bottleneck. Figure 3(h) shows that the normalized execution time is also nearly constant under different routing buffer capacities until which shrinks to 64 KB. Since the routing buffer is used to buffer the routing packets before they are sent, its capacity relies on the utilized network bandwidth and network latency.

4 MULTIGCN ARCHITECTURE

Guided by the above observations, we propose MultiGCN, an efficient MultiAccSys for large-scale GCNs that trades network latency for network bandwidth.

4.1 Architecture Overview

Figure 4 provides a illustration of the proposed architecture. Although MultiGCN does not rely on a particular network topology, we choose a 2D torus topology consisting of 16 processing nodes as our baseline, which is shown in Figure 4(a). By network links we refer to the NVLINK protocol, which is one of the most widely applied high-speed interconnection protocols and usually used between NVIDIA GPUs. A processing node, shown in Figure 4(b), is composed of a compute unit, a router, a receive unit, a send unit, an edge buffer, a scheduler, a loader, an aggregation buffer, a weight buffer, a combination buffer, and DRAM.

The compute unit consists of eight reusable 1×128 systolic arrays. Each processing element (PE) has four registers with two for input, one for output, and one for internal use respectively, and an ALU capable of multiplication and reduction (like MIN, MAX, ADD). The eight systolic arrays work separately, either in combination mode, like a traditional systolic array, or in aggregation mode. In aggregation mode, all PEs follow an identical three-stage pipeline: read two operands from the input registers, perform reduction, and write result to the output register. Moreover, a real-time scheduling of compute resources between aggregation and combination is implemented in MultiGCN, since all eight reusable systolic arrays can process workloads of both types. Note that

although a unified compute unit is used in this work, designs in other single-node accelerators can also be integrated for better efficiency or compatibility.

The router, receive unit, and send unit are used to transfer vertices' feature vectors and neighboring lists. The edge buffer and scheduler are used to efficiently organize computation. Each entry in the edge buffer contains the address of a vertex's feature vector in aggregation buffer and its neighbor list. The feature vector is read via address and aggregated into the intermediate result of vertices in the neighbor list. Process of aggregation is recorded aside the intermediate result in aggregation buffer. The weight buffer and combination buffer save the weight matrix and intermediate combination result for the combination process. The loader loads the meta-data of execution, ID and degree of vertices, feature vectors and edge lists, which the send unit and scheduler ingest to complete execution.

Topology-aware Multicast (Section 4.2). To reduce the requirement of network bandwidth, a topology-aware multicast mechanism with a one put per multicast message-passing model is proposed. Multicast is based on the simple concept that for vertex v , many processing nodes where v 's neighbors lie in can be satisfied by receiving the same packet containing a replica of v 's feature vector. To efficiently tailor multicast to the communication pattern of GCNs, we design our multicast to be network topology-aware and graph topology-aware. The network topology awareness helps route and split packets guided by routers' status and an explicit list of destination node ids in the packet. Thus, the packet can be quickly and exactly multicast to all destination nodes. The graph topology awareness is enabled by the offset list and neighbor lists in the packet which are used to exactly share a single replica to all neighbors in the same processing node. Although these capabilities introduce extra latency in the transmission because of the above additional info in packets, they help eliminate redundant transmissions and significantly reduce the need for network bandwidth.

Scatter-based Round Execution (Section 4.3). Although topology-aware multicast mechanism helps reduce the requirements of network bandwidth, its overhead is high for three reasons. *First*, a request-response loop, required by each replica's transmission, significantly increases the design complexity of MultiAccSys for the multicast mechanism. *Second*, the large info of the offset list and neighbor lists are coupled into a single packet, resulting in an unacceptable routing latency in multicast. *Third*, on-chip memory is unable to buffer total replicas of thousands of long feature vectors, which leads to frequent replacements of replicas between on-chip memory and off-chip memory. To this end, a scatter-based round execution mechanism is proposed, which inherently matches the behaviour of multicast. Specifically, each processing node scatters the replicas of vertices' feature vectors to remote processing nodes who perform aggregate function for these vertices' neighboring vertices, so that the request-response loop is eliminated. Besides, the graph is partitioned into multiple sub-graphs, each for one execution round. Thus, the large info of neighbor lists is partitioned and transmitted over several rounds, avoiding the unacceptable routing latency. Moreover, only a small number of replicas in each round are stored in on-chip memory until the corresponding round completes, reducing redundant off-chip memory accesses.

Algorithm 1: DyXY Routing Algorithm

```

1 foreach packet  $p$  to  $(x,y)$  in routing buffer do
2   ① if  $(x == Tx) \&\& (y == Ty)$  then
3     | receive  $p$  in current node  $(Tx, Ty)$ ;
4   end
5   ② else if  $(x == Tx) \parallel (y == Ty)$  then
6     | send  $p$  to neighbor on Y-axis or X-axis;
7   end
8   ③ else
9     | send  $p$  to neighbor with smallest stress value;
10  end
11 end

```

4.2 Topology-aware Multicast Mechanism

To enable efficient multicast, we propose a one put per multicast message-passing model based on the DyXY routing algorithm [23] to implement the multicast mechanism with the knowledge of network topology and graph topology.

One Put per Multicast. Our one put per multicast model is inspired by multicast on Ethernet. In Ethernet, multicast is group communication where data transmission is addressed to a group of destination computers simultaneously. In MultiGCN, put refers to putting the replica of a vertex's feature vector to its neighboring vertices, while multicast means the packet generated by put is scattered to all its destinations in the fashion of multicast.

The basic routing algorithm we use is DyXY [23], which provides adaptive routing based on congestion conditions nearby. The algorithm is adaptive in that it makes routing decisions by monitoring the congestion status nearby, and the deadlock-free and livelock-free features are reached by limiting the path of a packet in the network to one of the shortest paths between the source and the destination. If multiple shortest paths are available, the routers will help the packet to choose one of them based on the congestion condition of the network. A stress value, i.e., the occupation ratio of routing buffer, is used to represent the congestion condition of a router in this work. Each router stores instant stress values for all neighbors, which are updated periodically. The detailed routing algorithm is shown in Algorithm 1 and a routing example for the replica of V_0 's feature vector is depicted in Figure 5(a). See Section 4.3 for the details of graph mapping.

To couple the multicast mechanism with the DyXY routing algorithm, step ① in Algorithm 1 is modified to split packets as shown in Algorithm 2. Figure 5(b) presents the packet format used in Algorithm 2, which consists of four parts including the position of the next destination node (x, y) , network topology (neighbor-ID (nID) list and its size), graph topology (offset list, neighbor lists), and the replica of feature vector. In the line ② of Algorithm 2, all nIDs in nID list are transformed into the new coordinate $[x,y]$ by taking current node (Tx, Ty) as the Origin of coordinates and donated as a set $D = \{[x,y]\}$, when a packet arrives at the destination node (Tx, Ty) . Figure 5(c) gives an example for the transformation of nID, new node position $[x,y]$, and fixed node position (x,y) . In this example, $N_1 (1, 0)$ is taken as the Origin $[0,0]$, and the $[x,y]$ of its neighboring nodes are shown. In the line ③ to ⑫, based on the new coordinates, packet is partitioned into nine parts. Each part has a part of the nID list and neighbor lists, a new offset list, and a complete replica. In the line ⑭ to ④①, these nine parts are received by the current node or sent to the next destination node. Figure 5(d) gives a multicast example based on Algorithm 2 where the replica of V_0 's feature vector is multicast from N_1 to V_{35} and V_{51} in N_3 , V_{39} in N_7 , and V_{54} in

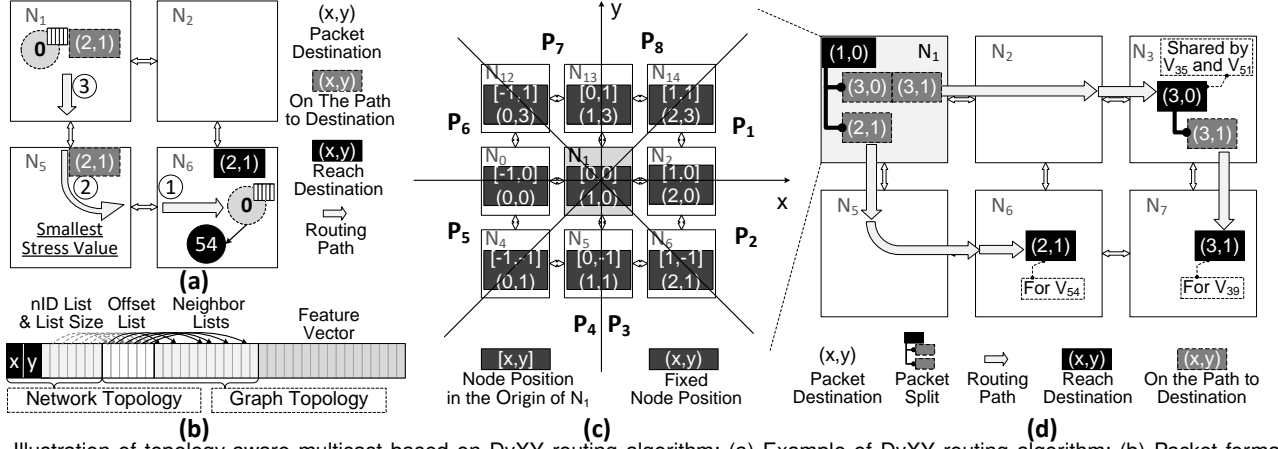


Fig. 5. Illustration of topology-aware multicast based on DyXY routing algorithm: (a) Example of DyXY routing algorithm; (b) Packet format for topology-aware multicast; (c) Packet split of topology-aware multicast in the step 1 of DyXY; (d) One possible multicast of V_0 's feature vector from N_1 (Origin) to V_{35} and V_{51} in N_3 , V_{39} in N_7 , and V_{54} in N_6 .

N_6 . Specifically, the packet arrives in N_1 (1,0) and then is split into two parts. One is P_3 and consists of one destination including [1, -1] (i.e., N_6 (2, 1)). The other one is P_2 and consists of two destination nodes including [2, 0] (i.e., N_3 (3, 0)) and [2, -1] (i.e., N_7 (3, 1)). Then, the former is sent to N_6 via N_5 . The latter is sent to N_3 via N_2 and is further multicast until the nID list in packet is empty. The packet received by N_3 is further shared by the aggregation of V_{35} and V_{51} indicated by the neighbor list in the packet. As a result, redundant transmissions are removed.

In this process, we have followed the spirit of trading latency for network bandwidth: although extra latencies in the transmission of packets are introduced for additional info, the topology-aware multicast mechanism alleviates the requirement of network bandwidth. However, this also introduces three inefficiencies: high design complexity, low utilization of compute resource, and redundant off-chip memory accesses. *First*, a request-response loop, required by each transmission of the replica, will significantly increase the design complexity. *Second*, the large size of neighbor lists in the packet causes intensive transmission and unacceptable routing latency, and most of the compute resources become under-utilized. *Third*, limited by the capacity of on-chip memory in each processing node, the large volume of received replicas need to be frequently moved between on-chip memory and off-chip memory. This is because thousands of replicas are received and shared by many vertices' aggregation in each processing node, but it takes a long time to process the long feature vectors, which means most of these replicas need to be first stored in off-chip memory and then reloaded when needed.

4.3 Scatter-based Round Execution Mechanism

To address the above inefficiencies, we propose a scatter-based round execution mechanism that well suits the topology-aware multicast mechanism. The key idea of the scatter-based round execution mechanism is simple but effective: we first partitions the graph into a set of sub-graphs and then processes one sub-graph per round. In each round, all replicas are kept on-chip until no longer needed. To improve resource utilization, we also implement intra- and inter-round overlaps.

Scatter or Gather. There are two ways to execute the aggregate function: the gather-based and scatter-based methods. As shown in Figure 6(a), in the gather-based method, each processing node (e.g., N_3 , N_6 , and N_7) first requests feature vectors of neighboring vertices (e.g., V_0) for each vertex (e.g., V_{35} ,

Algorithm 2: Packet Split of Multicast

```

1 ① if (x == Tx) && (y == Ty) then
2    transform nID list into  $D = \{[x, y]\}$  by taking node (Tx, Ty) as the Origin of coordinates;
3    split packet  $p$  into the following nine parts:
4     $P_0 = \{[0, 0]\} \cap D$ ;
5     $P_1 = \{[x, y] \mid y > 0, y \leq x\} \cap D$ ;
6     $P_2 = \{[x, y] \mid y \leq 0, y > -x\} \cap D$ ;
7     $P_3 = \{[x, y] \mid x > 0, y \leq -x\} \cap D$ ;
8     $P_4 = \{[x, y] \mid x \leq 0, y < x\} \cap D$ ;
9     $P_5 = \{[x, y] \mid y < 0, y \geq x\} \cap D$ ;
10    $P_6 = \{[x, y] \mid y \geq 0, y < -x\} \cap D$ ;
11    $P_7 = \{[x, y] \mid y \geq -x, x < 0\} \cap D$ ;
12    $P_8 = \{[x, y] \mid x \geq 0, y > x\} \cap D$ ;
13   receive and share  $P_0$  in current node (Tx, Ty);
14   if ( $P_1 \neq \emptyset$  && ( $P_2 \neq \emptyset$ )) then
15     send  $P_1 \cup P_2$  to  $[\text{MIN}(P_1.x \cup P_2.x), 0]$ ;
16   end
17   else
18     send  $P_1$  to  $[\text{MIN}(P_1.x), \text{MIN}(P_1.y)]$ ;
19     send  $P_2$  to  $[\text{MIN}(P_2.x), \text{MAX}(P_2.y)]$ ;
20   end
21   if ( $P_3 \neq \emptyset$  && ( $P_4 \neq \emptyset$ )) then
22     send  $P_3 \cup P_4$  to  $[0, \text{MAX}(P_3.y \cup P_4.y)]$ ;
23   end
24   else
25     send  $P_3$  to  $[\text{MIN}(P_3.x), \text{MAX}(P_3.y)]$ ;
26     send  $P_4$  to  $[\text{MAX}(P_4.x), \text{MAX}(P_4.y)]$ ;
27   end
28   if ( $P_5 \neq \emptyset$  && ( $P_6 \neq \emptyset$ )) then
29     send  $P_5 \cup P_6$  to  $[\text{MAX}(P_5.x \cup P_6.x), 0]$ ;
30   end
31   else
32     send  $P_5$  to  $[\text{MAX}(P_5.x), \text{MAX}(P_5.y)]$ ;
33     send  $P_6$  to  $[\text{MAX}(P_6.x), \text{MIN}(P_6.y)]$ ;
34   end
35   if ( $P_7 \neq \emptyset$  && ( $P_8 \neq \emptyset$ )) then
36     send  $P_7 \cup P_8$  to  $[0, \text{MIN}(P_7.y \cup P_8.y)]$ ;
37   end
38   else
39     send  $P_7$  to  $[\text{MAX}(P_7.x), \text{MIN}(P_7.y)]$ ;
40     send  $P_8$  to  $[\text{MIN}(P_8.x), \text{MIN}(P_8.y)]$ ;
41   end
42 end

```

V_{51} , V_{54} , and V_{39}) from the remote processing node (e.g., N_0) and then waits for the responses of feature vectors. Afterwards, the replicas of feature vectors are aggregated in the processing node of requester (e.g., N_3 , N_6 , and N_7). As a result, a request-response

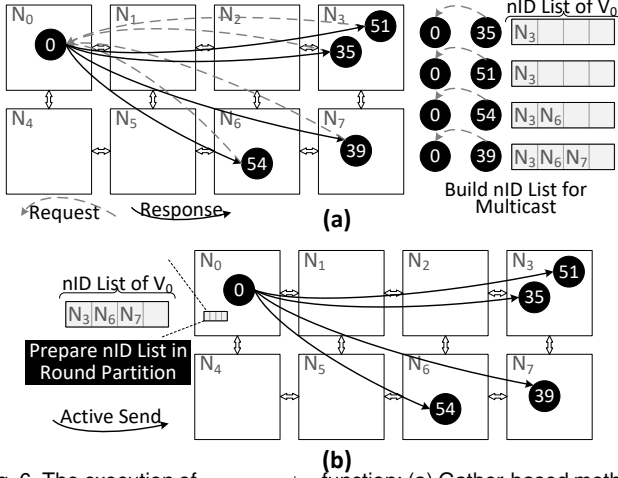


Fig. 6. The execution of aggregate function: (a) Gather-based method; (b) Scatter-based method.

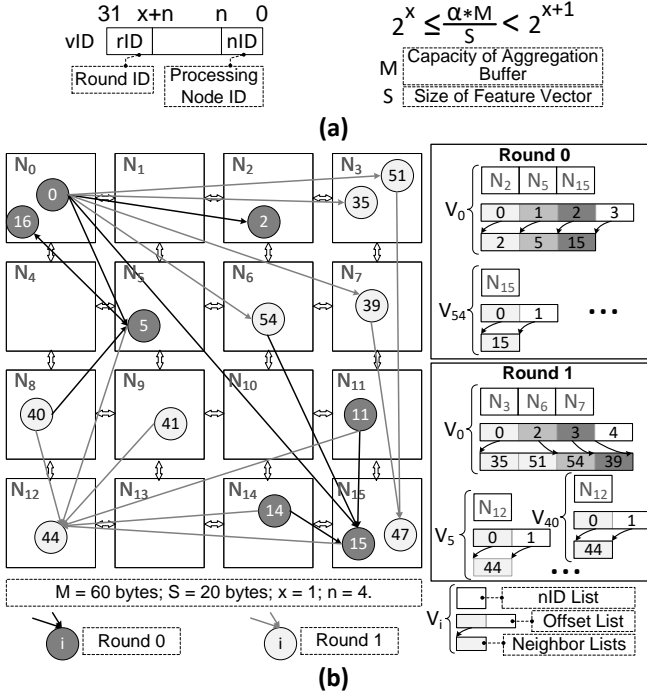


Fig. 7. Illustration of round partition: (a) Generation of round ID; (b) Example of round partition.

loop for each transmission of the replica is introduced. Besides, to support multicast, the remote processing node needs to collect request for each vertex's feature vector to build an nID list and then performs multicast based on this nID list.

As shown in Figure 6(b), in the scatter-based method, each processing node has an nID list derived from round partition (described in the next paragraph). Each processing node (e.g., N_0) actively sends the feature vector of each vertex (e.g., V_0) to the remote processing nodes (e.g., N_3 , N_6 , and N_7) where the outgoing neighboring vertices (e.g., V_{35} , V_{51} , V_{54} , and V_{39}) locate. Then, the feature vectors are aggregated in remote processing nodes. As a result, message passing only happens in a single direction. From the above, the scatter-based method inherently matches the behavior of topology-aware multicast mechanism, helping eliminate the request-response loop, and thus achieves lower design complexity than the gather-based method. Hence, MultiGCN employs the scatter-based method.

Round Partition and Execution. To avoid unacceptable routing latency and redundant off-chip memory accesses, a round exe-

Algorithm 3: Round Execution

```

1  load round info and configure round execution;
2  foreach vertex  $v$  in local do
3      load  $v$ 's feature vector, network topology, and graph topology;
4      if current node has  $v$ 's neighbor  $u$  then
5          save a replica in aggregation buffer;
6          save {buffer address, list of all neighbor  $u$ } to edge buffer;
7      end
8      send  $v$ 's data to remote processing nodes;
9  end

10 Receive
11 receive  $v$ 's feature vector and graph topology;
12 save a replica in aggregation buffer;
13 save {buffer address,  $v$ 's neighbors} to edge buffer;

14 Compute
15 perform aggregate function using buffer address and neighbors' vID in items of edge buffer;
16 perform combine function when aggregation is complete;
17 store final combined result to off-chip memory;

18 Synchronization
19 synchronize and complete the current round;

```

cution method coupled with a simple round partition is proposed. Figure 7 illustrates the round partition which is based on a simple graph mapping method to reduce the mapping overhead and simplify packet routing. As illustrated in Figure 7(a), for a vertex, the bits in range $[0, n]$ in the vertex ID (vID) will be the ID of the processing node to which the vertex is partitioned and mapped. The bits in range $[n, x+n]$ in the vID are used to partition and map 2^x vertices with interleaving vIDs into the same processing node together. The bits in range $[x+n, 32]$ in the vID will be the index of round (rID) for simplicity. The value of n is determined by the total number of processing nodes (#total_node) in MultiAccSys, which is equal to $\lfloor \log_2(\text{\#total_node}) \rfloor$. The value of x can be reconfigured for different datasets to better utilize on-chip memory, which is determined by $2^x \leq \frac{\alpha M}{S} < 2^{x+1}$, where M is the capacity of the aggregation buffer and S is the size of aggregated feature vector. The value of α requires to be less than 1 to spare space for network communication and rounds overlap. Therefore, the value of α is set to 0.75 in our implementation. For each vertex, all its incoming edges are partitioned into the same round, then used to build the nID list, offset list, and neighbor lists of its all in-coming neighboring vertices for multicast. The compressed sparse row format is used to reorganize the neighbor lists to reduce needs for both memory storage and network bandwidth. These information of each vertex is mapped into the same processing node with this vertex's feature vector. Note that after the round partition, if a vertex still has too many out-going neighbors in a round, this packet is further divided into several packets before sending to network. Figure 7(b) provides an example for round partition with $M = 60$ bytes, $S = 20$ bytes, $x = 1$, and $n = 4$. In this figure, a graph is *first* partitioned into two sub-graphs corresponding to two rounds. For example, V_{15} and V_{44} are partitioned into round 0 and round 1 with their in-coming edges, respectively. *Second*, the vID of each vertex (e.g., V_{15}) is included into the neighbor lists of its in-coming neighbors (e.g., V_0 and V_{54}) to support the scatter-based method. As a result, the large neighbor lists of high out-degree vertices (e.g. V_0) are sliced over several rounds, avoiding large info in a single packet.

Algorithm 3 demonstrates the round execution method which includes five steps: ① *Initialization*, where each processing node loads the round info and is configured for a new round. ② *Load and Send*, where each processing node loads graph data including feature vectors, graph topology, and network topology, and then sends the graph data to other nodes. ③ *Receive*, where each processing node receives the replica of feature vector and graph topology from remote nodes into the aggregation buffer and the edge buffer. ④ *Compute*, where each processing node executes the aggregate function or combine function to process graph data in local or from remote. ⑤ *Synchronization*, where each processing node broadcasts an end signal to others when its workload in the current round is completed, and the current round is terminated after total signals from other nodes are collected. Note that other synchronization mechanisms can also be used for better efficiency. Besides, execution overlap technique is utilized in the round execution to improve resource utilization. After step ①, the step ②, ③, and ④ can be overlapped intra round. Moreover, these three steps can also be overlapped inter round. Furthermore, the step ④ is able to actively process the graph data from local to keep compute resources busy when no graph data is received.

The round partition and round execution method provide two benefits. *First*, large neighbor lists are sliced, avoiding the compute resource underutilized due to the intensive transmission and unacceptable routing latency for a single packet. *Second*, the large volume of replicas is split and processed over a set of rounds, so that replicas in each round can be totally saved in on-chip memory, avoiding the frequent transfer of replicas between on-chip memory and off-chip memory.

5 EVALUATION METHODOLOGY

Evaluation Tools. We design and implement an in-house simulator to measure execution time in number of cycles. The simulator has a cycle-level model for many microarchitectural components, including multi-bank on-chip buffer, HBM (high bandwidth memory), NVLink, systolic arrays, and so on. To measure critical path delay (in cycles) of router, receive unit, send unit, loader, scheduler, and compute unit, we implement and synthesize these modules in Verilog. We use the Synopsys Design Compiler with the TSMC 12 nm standard VT library for the synthesis and estimate the power consumption using Synopsys PrimeTime PX. The slowest module has a critical path delay of 0.83 ns including the setup and hold time, putting MultiGCN comfortably at 1 GHz clock frequency. The access latency, energy, and area of the on-chip buffer and FIFO are estimated using Synopsys DesignWare Memory Compiler. The access latency and energy of HBM are simulated by Ramulator [24], a cycle-accurate DRAM simulator and estimated with 7 pJ/bit as in [25], respectively. The access latency and energy of NVLink are estimated with around 500 ns as in [26] and 8 pJ/bit as in [27], respectively.

Baselines and System Configurations. To demonstrate the advance of MultiGCN, we compare MultiGCN with a single-node GCN accelerator (i.e., AWB-GCN [15]) using identical hardware resources, two GPU-based solutions (i.e., PyG [29] and GNNAdvisor [30]) running on GPU T4, OPPE-based MulAccSys, and OPPE-based MulAccSys. Three configurations of MultiGCN are evaluated to assess MultiGCN. The first configuration is MultiGCN only employing the topology-aware multicast mechanism (TMM), denoted as **MultiGCN-TMM**. The second configuration

TABLE 2
System parameters of MultiGCN @1GHz & TSMC 12 nm.

| Network Parameters | | | |
|--|---------------------|--------------------|-----------------|
| Network Topology | #Processing Node | Network Bandwidth | Network Latency |
| 2D Torus | 16 | 600 GB/s | 500 Cycles |
| Memory Parameters of Each Processing Node | | | |
| Buffer in Router | Buffer in Send Unit | Buffer in Loader | Edge Buffer |
| 1.5 MB | 512 KB | 896 KB | 128 KB |
| Aggregation Buffer | Weight Buffer | Combination Buffer | HBM Bandwidth |
| 1 MB | 2 MB | 256 KB | 256 GB/s |
| Compute Parameters of Each Processing Node | | | |
| 8 Reusable Systolic Arrays (each size 1×128) | | | |

TABLE 3
Graph datasets used in evaluation [28].

| Name | $ V $ | $ E $ | d_v | $ h^0 $ | $ h^1 $ | Topology Size | Feature Size |
|-------------------|-------|-------|-------|---------|---------|---------------|--------------|
| Real-world Graphs | | | | | | | |
| Reddit (RD) | 233K | 114M | 489 | 602 | 128 | 460 MB | 561 MB |
| Orkut (OR) | 3M | 117M | 39 | 500 | 128 | 481 MB | 6 GB |
| LiveJournal (LJ) | 5M | 69M | 14 | 500 | 128 | 295 MB | 10 GB |
| Synthetic Graphs | | | | | | | |
| RMAT-19 (RM19) | 0.5M | 16.8M | 32 | 512 | 128 | 67 MB | 1 GB |
| RMAT-20 (RM20) | 1M | 33.6M | 32 | 512 | 128 | 134 MB | 2 GB |
| RMAT-21 (RM21) | 2.1M | 67.1M | 32 | 512 | 128 | 269 MB | 4 GB |
| RMAT-22 (RM22) | 4.2M | 134M | 32 | 512 | 128 | 537 MB | 8 GB |
| RMAT-23 (RM23) | 8.4M | 268M | 32 | 512 | 128 | 1074 MB | 16 GB |

is MultiGCN only employing the scatter-based round execution mechanism (SREM), denoted as **MultiGCN-SREM**. The last configuration is the MultiGCN employing both TMM and SREM, denoted as **MultiGCN-TMM+SREM**. All these configurations use the system parameters described in Table 2.

Workloads. We implement three well-known GCNs in MultiGCN, namely GCN [31], GINConv (GIN) [32], and GraphSage (SAG) [33]. Due to the long simulation time on large-scale graphs, we simulate only the first layer of these models. Since runtime characteristics of GCNs are input-dependent, we use several real-world and synthetic graphs as inputs to each GCN model, as shown in Table 3. Topology size of graph denotes the total size of edges, calculated as $|E| * 4$ Bytes. Feature size of graph denotes the total size of feature vectors, calculated as $|V| * |h^0| * 4$ Bytes.

6 RESULTS

6.1 Overall Results

Performance. Figure 8 compares the performance of the proposed MultiGCN against that of OPPE-based MulAccSys. In this figure, the last set of bars, labeled as GM, indicates geometric mean across all workloads. Our evaluation shows that MultiGCN with only TMM mechanism or only SREM mechanism outperforms OPPE-based MulAccSys by $2.9\times$ or $1.9\times$ on average. When both mechanisms are employed, MultiGCN achieves $4\sim 12\times$ speedup over OPPE-based MulAccSys, and $5.8\times$ on average.

To provide more insight into the performance improvement of MultiGCN, Table 4 shows the utilization ratios of network bandwidth, DRAM bandwidth, and compute unit in MultiGCN. Compared with OPPE-based MulAccSys, the utilization ratio of network bandwidth, DRAM bandwidth and compute unit of MultiGCN-TMM+SREM improve by $3.88\times$, $1.53\times$, and $7.33\times$ on average, respectively. This points the main contributor of the large speedup achieved by our design: the TMM mechanism and the SREM mechanism.

Area and Power. Table 5 gives the detailed characteristics of MultiGCN. The area and power of each processing node are 12.4 mm^2 and 3671.13 mW respectively. The buffers including edge buffer, aggregation buffer, weight buffer, and combination buffer occupy most area of the processing node and accounts for 48% power of the processing node. The area and power produced

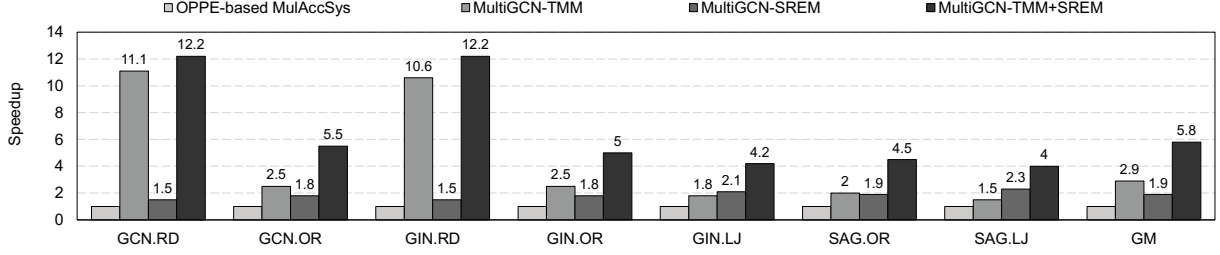


Fig. 8. Performance comparison between OPPE-based MulAccSys and MultiGCN (normalized to OPPE-based MulAccSys).

TABLE 4

Utilization ratio (%) of network bandwidth, dram bandwidth, and compute unit of OPPE-based MulAccSys and MultiGCN.

| | OPPE-based MulAccSys | | | MultiGCN-TMM | | | MultiGCN-SREM | | | MultiGCN-TMM+SREM | | |
|--------|----------------------|----------------|--------------|-------------------|----------------|--------------|-------------------|----------------|--------------|-------------------|----------------|--------------|
| | Network Bandwidth | DRAM Bandwidth | Compute Unit | Network Bandwidth | DRAM Bandwidth | Compute Unit | Network Bandwidth | DRAM Bandwidth | Compute Unit | Network Bandwidth | DRAM Bandwidth | Compute Unit |
| GCN.RD | 19 | 12 | 2 | 4 | 29 | 20 | 28 | 17 | 3 | 87 | 14 | 22 |
| GCN.OR | 17 | 15 | 6 | 6 | 41 | 16 | 31 | 20 | 12 | 69 | 32 | 35 |
| GCN.LJ | 16 | 20 | 14 | 7 | 41 | 26 | 34 | 23 | 30 | 60 | 31 | 68 |
| GIN.RD | 19 | 12 | 2 | 4 | 21 | 21 | 28 | 17 | 3 | 87 | 14 | 24 |
| GIN.OR | 17 | 15 | 8 | 6 | 41 | 21 | 31 | 19 | 15 | 62 | 29 | 41 |
| GIN.LJ | 15 | 19 | 19 | 7 | 41 | 34 | 33 | 22 | 40 | 51 | 26 | 80 |
| SAG.RD | 19 | 19 | 9 | 8 | 39 | 17 | 45 | 29 | 20 | 76 | 36 | 39 |
| SAG.OR | 16 | 18 | 10 | 7 | 42 | 21 | 31 | 21 | 20 | 60 | 31 | 46 |
| SAG.LJ | 15 | 23 | 21 | 8 | 40 | 32 | 34 | 24 | 47 | 53 | 30 | 84 |
| GM | 17 | 17 | 8 | 6 | 37 | 22 | 33 | 21 | 15 | 66 | 26 | 44 |

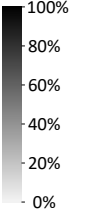


TABLE 5

Characteristics of processing node @1GHz & TSMC 12 nm.

| Component or Block | Area (mm ²) | % | Power (mW) | % |
|-------------------------------|-------------------------|-------|------------|-------|
| Processing Node | 12.4 | 100 | 3671.13 | 100 |
| Breakdown by Functional Block | | | | |
| Edge Buffer | 0.23 | 1.88 | 9.03 | 0.25 |
| Aggregation Buffer | 1.87 | 15.06 | 578.3 | 15.75 |
| Weight Buffer | 3.74 | 30.11 | 614.13 | 16.73 |
| Combination Buffer | 0.47 | 3.76 | 551.42 | 15.02 |
| Compute Unit | 0.84 | 6.8 | 650.63 | 17.72 |
| Router | 2.8 | 22.59 | 689.45 | 18.78 |
| Loader | 1.52 | 12.24 | 320.51 | 8.73 |
| Send Unit | 0.93 | 7.53 | 257.6 | 7.02 |
| Scheduler | 4.73E-04 | 0.00 | 0.00 | 0.00 |
| Others | 1.89E-03 | 0.02 | 0.04 | 0.00 |

TABLE 6

Normalized network transmission and DRAM access of MultiGCN (normalized to OPPE-based MulAccSys).

| | MultiGCN-TMM | | MultiGCN-SREM | | MultiGCN-TMM+SREM | |
|--------|--------------|--------|---------------|--------|-------------------|--------|
| | Trans. | Access | Trans. | Access | Trans. | Access |
| GCN.RD | 2% | 21% | 100% | 93% | 37% | 10% |
| GCN.OR | 14% | 112% | 100% | 72% | 75% | 39% |
| GCN.LJ | 25% | 114% | 100% | 53% | 79% | 33% |
| GIN.RD | 2% | 16% | 100% | 93% | 37% | 10% |
| GIN.OR | 14% | 112% | 100% | 72% | 75% | 39% |
| GIN.LJ | 25% | 118% | 100% | 53% | 79% | 33% |
| SAG.RD | 20% | 102% | 100% | 63% | 88% | 41% |
| SAG.OR | 22% | 116% | 100% | 60% | 81% | 38% |
| SAG.LJ | 35% | 115% | 100% | 48% | 86% | 33% |
| GM | 13% | 75% | 100% | 66% | 68% | 27% |

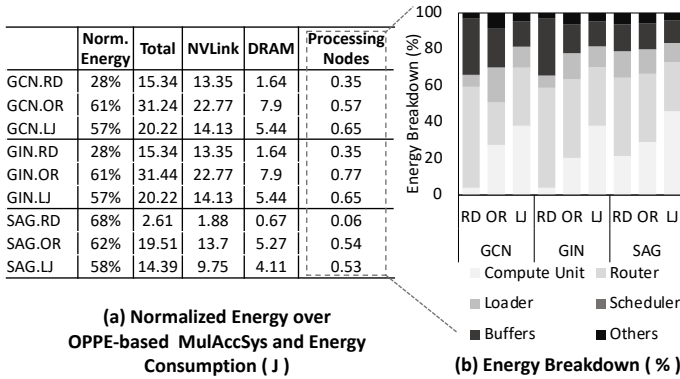


Fig. 9. Energy: (a) Normalized energy over OPPE-based MulAccSys and energy details; (b) Energy breakdown of processing nodes.

by the compute unit are 6.8% and 17.72%. For the computation precision, we use 32-bit fixed point which is enough to maintain the accuracy of GCN inference. The area and power produced by router are 22.59% and 18.78% due to the large routing buffer and packet transmission.

Energy and its Breakdown. Figure 9 shows the energy consumption of MultiGCN-TMM+SREM in details. Figure 9(a) depicts that MultiGCN costs only 28%~68% energy of OPPE-based MulAccSys. The energy consumed by network (i.e., NVLink) is larger than DRAM and processing nodes in all cases, since the feature vector loaded from DRAM can be shared across multiple remote processing nodes. Figure 9(b) shows that compute unit, router and buffers consume most energy of the processing nodes.

6.2 Effect and Overhead of Optimizations

To dissect the effect of our optimizations, the normalized network transmission and DRAM access of MultiGCN (normalized to OPPE-based MulAccSys) are shown in Table 6. The reductions of redundant transmissions and DRAM accesses as well as the overhead analysis of these optimizations are also shown in Table 7.

Effect. The TMM mechanism helps eliminate the redundant transmissions. Table 6 shows that the network transmission of MultiGCN-TMM is only 13% of OPPE-based MulAccSys. This is because a single packet containing a replica of the feature vector is sent to many other processing nodes that request it via multicast. Note that the number of DRAM access in RD dataset decreases, but extra DRAM accesses are introduced in most datasets. This is because a feature vector in RD dataset loaded from DRAM can be shared by many remote processing nodes due to its extremely high average degree (i.e., 489). The SREM mechanism avoids the frequent transfer of replicas between on-chip memory and off-chip memory. Specifically, the rounds are properly partitioned so that the replicas of all vertices and intermediate results in a round always stays on-chip until the computation is done. Compared with OPPE-based MulAccSys, MultiGCN-SREM introduces only 66% number of DRAM accesses on average.

Table 6 shows that when these two mechanisms are employed, both the network transmission and DRAM accesses are reduced significantly to only 68% and 27% on average, respectively. Note that the effect of TMM mechanism is hurt by the SREM mechanism because each round may introduce a multicast of the

TABLE 7

Reductions of redundant transmission and redundant DRAM access, extra transmission latency, and extra preprocessing time compared with OPPE-based MulAccSys.

| MultiGCN-TMM+SREM | | | | |
|-------------------|------------------------|-----------------------|----------------------|----------------------|
| | Redundant Transmission | Redundant DRAM access | Transmission Latency | Round Partition Time |
| GCN.RD | -64% | -100% | +0.52% | +6.6% |
| GCN.OR | -30% | -100% | +0.15% | +12% |
| GCN.LJ | -30% | -100% | +0.13% | +2.8% |
| GIN.RD | -64% | -100% | +0.52% | +6.6% |
| GIN.OR | -30% | -100% | +0.15% | +12% |
| GIN.LJ | -30% | -100% | +0.13% | +2.8% |
| SAG.RD | -17% | -100% | +0.07% | +6.6% |
| SAG.OR | -25% | -100% | +0.11% | +12% |
| SAG.LJ | -24% | -100% | +0.1% | +2.8% |
| GM | -32% | -100% | +0.21% | +6.1% |

same feature vector. In contrast, TMM mechanism promotes the effect of SREM mechanism since a feature vector loaded from DRAM can be multicast to and shared by many remote processing nodes. Table 7 depicts that MultiGCN-TMM+SREM reduces 32% redundant network transmissions and 100% of redundant DRAM accesses on average compared to OPPE-based MulAccSys.

Overhead. The main optimization overheads are the extras of transmission latency and preprocessing time for round partition, but all of them are small, only 0.21% and 6.1% on average, as shown in the last two columns in Table 7. Note that as the reduction of redundant transmissions increases, the network topology and graph topology information in the packet increases transmission latency. The round partition accounts for less than 12% time of the graph mapping because it can be coupled into the process of graph mapping. Besides, it is a one-time overhead for each dataset that can be amortized over the execution of different GCN models.

6.3 Comparisons with the State of the Arts

The performance of MultiGCN (1 node) is slightly lower than that of GNNAdvisor running in one GPU T4, $0.7\times$ on average. However, MultiGCN aims to scale single-node accelerator to accelerate GCNs on large-scale graphs efficiently, such as average $3.4\times$ speedup of MultiGCN (4 nodes) over GNNAdvisor.

To demonstrate the advance of MultiGCN, we compare MultiGCN against the state of the arts. Figure 10(a) shows that the average speedup of MultiGCN (1 node) is slightly lower than that of AWB-GCN and GNNAdvisor. However, MultiGCN aims to scale single-node accelerator to accelerate GCNs on large-scale graphs efficiently, such as average $4\times$ and $3.4\times$ speedup of MultiGCN (4 nodes) over AWB-GCN and GNNAdvisor respectively. Moreover, the peak performance, DRAM bandwidth, and maximum power of MultiGCN (1 node) are respectively only 25%, 85%, and 5% of GPU T4. MultiGCN (4 nodes) achieves average $4\times$ speedup over PyG with 4 GPU T4. This is because GPUs aim at workloads with regular execution pattern, but they cannot efficiently tackle irregular execution patterns of GCNs [11], [15], [16], [34], [35]. Note that GPU performance of PyG is estimated by accumulating the kernel execution time which eliminates the memory copy time and system stack overhead. Besides, PyG leverages mini-batch to make each GPU executes inference independently, so that inter-GPU communications are eliminated. But mini-batch multiplies data volume in system due to massive copies of neighboring feature vectors in each GPU. Figure 10(b) shows that MultiGCN (128 nodes and 8 TOPS) achieves average $9.6\times$ and $2.3\times$ speedup over OPPE-based MulAccSys (128 nodes and 8 TOPS) and OPPE-based MulAccSys (128 nodes and 8 TOPS) respectively due to less network transmissions and DRAM accesses. MultiGCN has

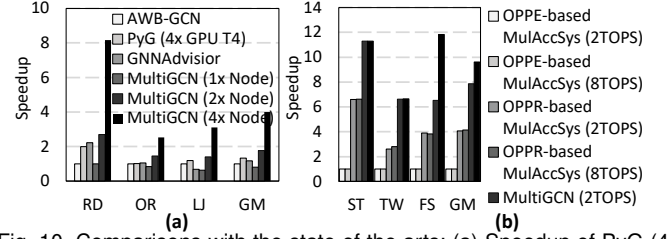


Fig. 10. Comparisons with the state of the arts: (a) Speedup of PyG (4 GPU T4), GNNAdvisor (1 GPU T4), MultiGCN (2 nodes), and MultiGCN (4 nodes) over AWB-GCN; (b) Speedup of MultiGCN (128 nodes) over OPPE-based and OPPE-based MulAccSys (128 nodes).

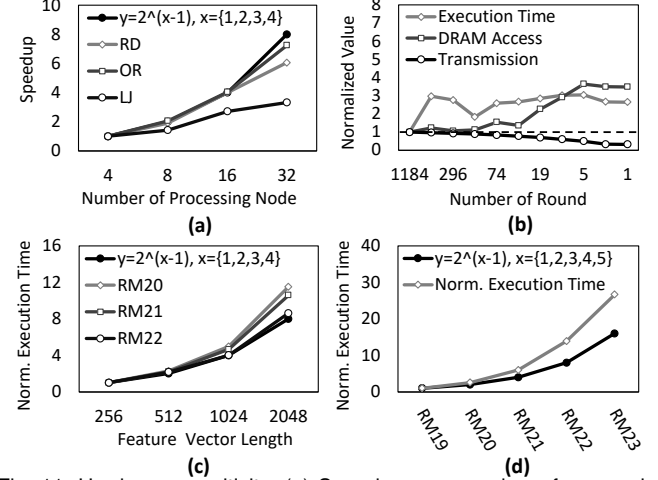


Fig. 11. Hardware sensitivity: (a) Speedup over number of processing node; (b) Normalized execution time, normalized amount of network transmission, and normalized amount of DRAM access across number of round. Graph characteristics sensitivity: Normalized execution time across (c) feature vector length and (d) vertex scale.

different speedup on FS dataset when compute capability increases because the number of network transmissions of FS is little while the number of compute for local data processing is large.

6.4 Exploration of Design

We conduct several experiments on GCN model to explore our architecture design in terms of hardware sensitivity and graph characteristic sensitivity as follows. Due to the long simulation time, we simulate the processing of 10% number of vertices for each experiment in this subsection.

Hardware Sensitivity. *First*, Figure 11(a) illustrates the speedup across different number of nodes of 2D torus network topology. MultiGCN gains performance improvement on RD and OR datasets as the number of nodes increases, and the speedup remains linear as the number of nodes increase to 32. Limited by the network bandwidth, the performance gain on LJ dataset gradually decreases as the number of node increases. This is due to the low reusability of feature vector in the network transmission since the average vertex degree of LJ dataset is low. *Second*, Figure 11(b) shows that the amount of network transmission decreases as the number of round decreases in the processing of LJ dataset because the number of multicast for the same feature vector decreases. Besides, the execution time and number of DRAM accesses are variable across different numbers of round. This leaves room for further optimizing the design to fit different requirements, which will be explored in our future work.

Graph Characteristic Sensitivity. *First*, the length of feature vector (i.e., $|h^0|$) doubles in Figure 11(c), which means the amount of workload in both the Aggregation phase and Combination phase double, and network transmission

increases even more. However, the execution time increase to more than $2\times$. In particular, the performance is sensitive to the length of the feature vector, which is mainly because the more network transmission imposes more pressure on network. *Second*, the number of vertex in graph doubles in Figure 11(d), which means the amount of workload in both the Aggregation phase and Combination phase and network transmission doubles too. However, the execution time increase to more than $2\times$. That is, the performance is sensitive to the vertex scale, since the large vertex scale with the same average degree increases the sparsity of graph, which hinders the performance.

7 RELATED WORK

Many software frameworks for GCNs have been developed to release the programming efforts while improving performance on modern architectures [1], [29], [36]. For example, PyG [29] is built upon PyTorch to easily program GNNs. It consists of easy-to-use mini-batch loaders for operating on giant graphs and multi-GPU support. Unfortunately, the distinct execution pattern in GCNs causes processing inefficiencies on conventional architectures. GCNs demand specialized architecture design.

Hardware acceleration for GCNs has been recently explored. Many single-node domain-specific architectures and frameworks have been designed for GCN acceleration [11], [15]–[17], [37]–[42]. For example, HyGCN [11] proposes a hybrid architecture to address the hybrid execution pattern of GCNs. However, the ever-growing scale of graphs has imposed new challenges that such accelerators cannot sufficiently address. Therefore, a multi-node acceleration system is highly desired.

Although a straightforward multi-node design for large-scale GCNs follows Tesseract or other Tesseract-based architectures [20], [21], [43], it suffers from two inefficiencies including a vast of redundant transmissions and redundant off-chip memory accesses. Therefore, we propose MultiGCN, an efficient Multi-AccSys for large-scale GCNs.

8 CONCLUSION

In this work, we aim to scale the single-node GCN accelerator to accelerate GCNs on large-scale graphs. We first identify the communication pattern and challenges of the multi-node acceleration for GCNs. Guided by the observations in characterization, we then propose MultiGCN, an efficient MultiAccSys for large-scale GCNs that trades network latency for network bandwidth. MultiGCN achieves $4\sim 12\times$ and $2.5\sim 8\times$ speedup over baseline MultiAccSys and multi-GPU solution respectively.

REFERENCES

- [1] H. Yang, “Aligraph: A comprehensive graph neural network platform,” in *Proceedings of the 25th ACM SIGKDD International Conference on Knowledge Discovery & Data Mining*, 2019, pp. 3165–3166.
- [2] Z. Wu, S. Pan, F. Chen, G. Long, C. Zhang, and S. Y. Philip, “A comprehensive survey on graph neural networks,” *IEEE transactions on neural networks and learning systems*, vol. 32, no. 1, pp. 4–24, 2020.
- [3] J. Zhou, G. Cui, S. Hu, Z. Zhang, C. Yang, Z. Liu, L. Wang, C. Li, and M. Sun, “Graph neural networks: A review of methods and applications,” *AI Open*, vol. 1, pp. 57–81, 2020.
- [4] Z. Zhang, P. Cui, and W. Zhu, “Deep learning on graphs: A survey,” *IEEE Transactions on Knowledge and Data Engineering*, 2020.
- [5] M. M. Bronstein, J. Bruna, Y. LeCun, A. Szlam, and P. Vandergheynst, “Geometric deep learning: going beyond euclidean data,” *IEEE Signal Processing Magazine*, vol. 34, no. 4, pp. 18–42, 2017.
- [6] M. Schlichtkrull, T. N. Kipf, P. Bloem, R. Van Den Berg, I. Titov, and M. Welling, “Modeling relational data with graph convolutional networks,” in *European Semantic Web Conference*. Springer, 2018, pp. 593–607.
- [7] R. Ying, R. He, K. Chen, P. Eksombatchai, W. L. Hamilton, and J. Leskovec, “Graph convolutional neural networks for web-scale recommender systems,” in *Proceedings of the 24th ACM SIGKDD International Conference on Knowledge Discovery & Data Mining*, 2018, pp. 974–983.
- [8] X. Chen, L.-J. Li, L. Fei-Fei, and A. Gupta, “Iterative visual reasoning beyond convolutions,” in *Proceedings of the IEEE Conference on Computer Vision and Pattern Recognition*, 2018, pp. 7239–7248.
- [9] L. Oliver and P. Luis, “Traffic prediction with advanced graph neural networks.” [Online]. Available: <https://deeppmind.com/blog/article/traffic-prediction-with-advanced-graph-neural-networks>
- [10] Y. Ma, H. Ren, B. Khailany, H. Sikka, L. Luo, K. Natarajan, and B. Yu, “High performance graph convolutional networks with applications in testability analysis,” in *2019 56th ACM/IEEE Design Automation Conference (DAC)*, June 2019, pp. 1–6.
- [11] M. Yan, L. Deng, X. Hu, L. Liang, Y. Feng, X. Ye, Z. Zhang, D. Fan, and Y. Xie, “Hygcen: A gcen accelerator with hybrid architecture,” in *2020 IEEE International Symposium on High Performance Computer Architecture (HPCA)*. IEEE, 2020, pp. 15–29.
- [12] M. Yan, Z. Chen, L. Deng, X. Ye, Z. Zhang, D. Fan, and Y. Xie, “Characterizing and understanding gcns on gpu,” *IEEE Computer Architecture Letters*, vol. 19, no. 1, pp. 22–25, 2020.
- [13] E. Lindholm, J. Nickolls, S. Oberman, and J. Montrym, “Nvidia tesla: A unified graphics and computing architecture,” *IEEE micro*, vol. 28, no. 2, pp. 39–55, 2008.
- [14] H. Zeng and V. Prasanna, “Graphact: Accelerating gcen training on cpu-fpga heterogeneous platforms,” in *The 2020 ACM/SIGDA International Symposium on Field-Programmable Gate Arrays*, 2020, pp. 255–265.
- [15] T. Geng, A. Li, R. B. Shi, C. S. Wu, T. Q. Wang, Y. F. Li, P. Haghi, A. Tumeo, S. Che, S. Reinhardt, and M. C. Herboldt, “Awb-gcn: A graph convolutional network accelerator with runtime workload rebalancing,” in *2020 53rd Annual IEEE/ACM International Symposium on Microarchitecture (MICRO)*, Oct. 2020.
- [16] S. Liang, Y. Wang, C. Liu, L. He, L. Huawei, D. Xu, and X. Li, “Engn: A high-throughput and energy-efficient accelerator for large graph neural networks,” *IEEE Transactions on Computers*, 2020.
- [17] J. Li, A. Louri, A. Karanth, and R. Bunescu, “Gcnax: A flexible and energy-efficient accelerator for graph convolutional neural networks,” in *2021 IEEE International Symposium on High-Performance Computer Architecture (HPCA)*. IEEE, 2021, pp. 775–788.
- [18] W. Hu, M. Fey, M. Zitnik, Y. Dong, H. Ren, B. Liu, M. Catasta, and J. Leskovec, “Open graph benchmark: Datasets for machine learning on graphs,” *arXiv preprint arXiv:2005.00687*, 2020.
- [19] N. P. Jouppi, D. H. Yoon, G. Kurian, S. Li, N. Patil, J. Laudon, C. Young, and D. Patterson, “A domain-specific supercomputer for training deep neural networks,” *Communications of the ACM*, vol. 63, no. 7, pp. 67–78, 2020.
- [20] J. Ahn, S. Hong, S. Yoo, O. Mutlu, and K. Choi, “A scalable processing-in-memory accelerator for parallel graph processing,” in *Proceedings of the 42nd Annual International Symposium on Computer Architecture*, 2015, pp. 105–117.
- [21] M. Zhang, Y. Zhuo, C. Wang, M. Gao, Y. Wu, K. Chen, C. Kozyrakis, and X. Qian, “Graphp: Reducing communication for pim-based graph processing with efficient data partition,” in *2018 IEEE International Symposium on High Performance Computer Architecture (HPCA)*. IEEE, 2018, pp. 544–557.
- [22] A. Li, S. L. Song, J. Chen, J. Li, X. Liu, N. R. Tallent, and K. J. Barker, “Evaluating modern gpu interconnect: Pcie, nvlink, nv-sli, nvswitch and gpubdirect,” *IEEE Transactions on Parallel and Distributed Systems*, vol. 31, no. 1, pp. 94–110, 2019.
- [23] M. Li, Q.-A. Zeng, and W.-B. Jone, “Dyxy: A proximity congestion-aware deadlock-free dynamic routing method for network on chip,” in *Proceedings of the 43rd Annual Design Automation Conference*, ser. DAC ’06. New York, NY, USA: Association for Computing Machinery, 2006, p. 849–852. [Online]. Available: <https://doi.org/10.1145/1146909.1147125>
- [24] Y. Kim, W. Yang, and O. Mutlu, “Ramulator: A fast and extensible dram simulator,” *IEEE Comput. Archit. Lett.*, vol. 15, no. 1, pp. 45–49, Jan. 2016.
- [25] M. O’Connor, “Highlights of the high-bandwidth memory (hbm) standard,” in *Memory Forum Workshop*, 2014.
- [26] C. Lutz, S. Breß, S. Zeuch, T. Rabl, and V. Markl, “Pump up the volume: Processing large data on gpus with fast interconnects,” in *Proceedings*

of the 2020 ACM SIGMOD International Conference on Management of Data, 2020, pp. 1633–1649.

- [27] D. BILL. Gtc china 2020 keynote. [Online]. Available: https://live.nvidia-china.com/20201215-gtc-china-2020/deck-assets/GTC_China_2020_Keynote.pdf
- [28] J. Leskovec and A. Krevl, “SNAP Datasets: Stanford large network dataset collection,” <http://snap.stanford.edu/data>, Jun. 2014.
- [29] M. Fey and J. E. Lenssen, “Fast graph representation learning with PyTorch Geometric,” in *ICLR Workshop on Representation Learning on Graphs and Manifolds*, 2019.
- [30] Y. Wang, B. Feng, G. Li, S. Li, L. Deng, Y. Xie, and Y. Ding, “Gnnadviser: An adaptive and efficient runtime system for {GNN} acceleration on gpus,” in *15th {USENIX} Symposium on Operating Systems Design and Implementation ({OSDI} 21)*, 2021, pp. 515–531.
- [31] T. N. Kipf and M. Welling, “Semi-supervised classification with graph convolutional networks,” *CoRR*, vol. abs/1609.02907, 2016. [Online]. Available: <http://arxiv.org/abs/1609.02907>
- [32] K. Xu, W. Hu, J. Leskovec, and S. Jegelka, “How powerful are graph neural networks?” *CoRR*, vol. abs/1810.00826, 2018. [Online]. Available: <http://arxiv.org/abs/1810.00826>
- [33] W. Hamilton, Z. Ying, and J. Leskovec, “Inductive representation learning on large graphs,” in *Advances in Neural Information Processing Systems 30*, 2017, pp. 1024–1034. [Online]. Available: <http://papers.nips.cc/paper/6703-inductive-representation-learning-on-large-graphs.pdf>
- [34] M. Yan, X. Hu, S. Li, A. Basak, H. Li, X. Ma, I. Akgun, Y. Feng, P. Gu, L. Deng, X. Ye, Z. Zhang, D. Fan, and Y. Xie, “Alleviating irregularity in graph analytics acceleration: A hardware/software co-design approach,” in *Proceedings of the 52Nd Annual IEEE/ACM International Symposium on Microarchitecture*, ser. MICRO ’52. New York, NY, USA: ACM, 2019, pp. 615–628. [Online]. Available: <http://doi.acm.org/10.1145/3352460.3358318>
- [35] T. J. Ham, L. Wu, N. Sundaram, N. Satish, and M. Martonosi, “Graphicionado: A high-performance and energy-efficient accelerator for graph analytics,” in *2016 49th Annual IEEE/ACM International Symposium on Microarchitecture (MICRO)*, Oct. 2016, pp. 1–13.
- [36] Deep graph library. [Online]. Available: <https://docs.dgl.ai>
- [37] X. Chen, Y. Wang, X. Xie, X. Hu, A. Basak, L. Liang, M. Yan, L. Deng, Y. Ding, Z. Du, and Y. Xie, “Rubik: A hierarchical architecture for efficient graph neural network training,” *IEEE Transactions on Computer-Aided Design of Integrated Circuits and Systems*, pp. 1–1, 2021.
- [38] B. Zhang, R. Kannan, and V. Prasanna, “Boostgcn: A framework for optimizing gcn inference on fpga,” in *2021 IEEE 29th Annual International Symposium on Field-Programmable Custom Computing Machines (FCCM)*. IEEE, 2021, pp. 29–39.
- [39] J. R. Stevens, D. Das, S. Avancha, B. Kaul, and A. Raghunathan, “Gnenerator: A hardware/software framework for accelerating graph neural networks,” *arXiv preprint arXiv:2103.10836*, 2021.
- [40] S. Mondal, S. D. Manasi, K. Kunal, and S. S. Sapatnekar, “Gnnie: Gnn inference engine with load-balancing and graph-specific caching,” *arXiv preprint arXiv:2105.10554*, 2021.
- [41] Z. Zhou, S. Bizhao, Z. Zhang, G. Yijin, S. Guangyu, and L. Guojie, “Blockgcn: Towards efficient GNN acceleration using block-circulant weight matrices,” in *2021 58th ACM/IEEE Design Automation Conference (DAC)*. IEEE, 2021.
- [42] T. Geng, C. Wu, Y. Zhang, C. Tan, C. Xie, H. You, M. Herbordt, Y. Lin, and A. Li, “I-gcn: A graph convolutional network accelerator with runtime locality enhancement through islandization,” in *MICRO-54: 54th Annual IEEE/ACM International Symposium on Microarchitecture*, 2021, pp. 1051–1063.
- [43] Y. Zhuo, C. Wang, M. Zhang, R. Wang, D. Niu, Y. Wang, and X. Qian, “Graphq: Scalable pim-based graph processing,” in *Proceedings of the 52nd Annual IEEE/ACM International Symposium on Microarchitecture*, 2019, pp. 712–725.



Gongjian Sun received the B.S. degree from University of Chinese Academy of Sciences, Beijing, China in 2019. He is currently a post-graduate at Institute of Computing Technology, Chinese Academy of Sciences, Beijing, China. His current research interests include high-throughput computer architecture and graph-based hardware accelerator.



Mingyu Yan received his Ph.D. degree from University of Chinese Academy of Sciences, Beijing, China in 2020. He is currently an Assistant Professor at Institute of Computing Technology, Chinese Academy of Sciences, Beijing, China. His current research interests include graph-based hardware accelerator and high-throughput computer architecture.



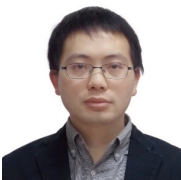
Duo Wang received his B.S. degree from Southeast University, Nanjing, China in 2018. He is currently a Ph.D. candidate at Institute of Computing Technology, Chinese Academy of Sciences, Beijing, China. His current research interests include high-performance computer architecture and software simulation.



Han Li received the B.S. degree from Jilin University, Changchun, China in 2016. She is currently a Ph.D. candidate at Institute of Computing Technology, Chinese Academy of Sciences, Beijing, China. Her current research interests include computer architecture and graph-based hardware accelerator.



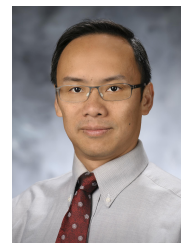
Wenming Li received the Ph.D. degree in computer architecture from Institute of Computing Technology, Chinese Academy of Sciences, Beijing, in 2016. He is currently an associate professor in Institute of Computing Technology, Chinese Academy of Sciences, Beijing. His main research interests include high-throughput processor architecture, dataflow architecture and software simulation.



Xiaochun Ye received his Ph.D. degree in computer architecture from Institute of Computing Technology, Chinese Academy of Sciences, Beijing, in 2010. He is currently an associate professor in Institute of Computing Technology, Chinese Academy of Sciences, Beijing. His main research interests include high-performance computer architecture and software simulation.



Dongrui Fan received his Ph.D. degree in computer architecture from Institute of Computing Technology, Chinese Academy of Sciences, Beijing, in 2005. He is currently a professor and Ph.D. supervisor in Institute of Computing Technology, Chinese Academy of Sciences, Beijing. His main research interests include high-throughput computer architecture and high-performance computer architecture.



Yuan Xie received his Ph.D. degrees from Electrical Engineering Department, Princeton University, Princeton, NJ, USA in 2002. He was a Professor with Pennsylvania State University, State College, PA, USA, from 2003 to 2014. He is currently a Professor with the Department of Electrical and Computer Engineering, University of California at Santa Barbara, Santa Barbara, CA, USA.